J. Phycol. **52,** 161–173 (2016)

DOI: 10.1111/jpy.12392

ARAGONITE INFILL IN OVERGROWN CONCEPTACLES OF CORALLINE *LITHOTHAMNION* SPP. (HAPALIDIACEAE, HAPALIDIALES, RHODOPHYTA): NEW INSIGHTS IN BIOMINERALIZATION AND PHYLOMINERALOGY[1]

Sherry Krayesky-Self,[2] *Joseph L. Richards*

University of Louisiana at Lafayette, Lafayette, Louisiana 70504-3602, USA

Mansour Rahmatian

Core Mineralogy Inc., Lafayette, Louisiana 70506, USA

and Suzanne Fredericq

University of Louisiana at Lafayette, Lafayette, Louisiana 70504-3602, USA

New empirical and quantitative data in the study of calcium carbonate biomineralization and an expanded coralline *psb*A framework for phylomineralogy are provided for crustose coralline red algae. Scanning electron microscopy (SEM) and energy dispersive spectrometry (SEM-EDS) pinpointed the exact location of calcium carbonate crystals within overgrown reproductive conceptacles in rhodolith-forming *Lithothamnion* species from the Gulf of Mexico and Pacific Panama. SEM-EDS and X-ray diffraction (XRD) analysis confirmed the elemental composition of these calcium carbonate crystals to be aragonite. After spore release, reproductive conceptacles apparently became overgrown by new vegetative growth, a strategy that may aid in sealing the empty conceptacle chamber, hence influencing the chemistry of the microenvironment and in turn promoting aragonite crystal growth. The possible relevance of various types of calcium carbonate polymorphs present in the complex internal structure and skeleton of crustose corallines is discussed. This is the first study to link SEM, SEM-EDS, XRD, Microtomography and X-ray microscopy data of aragonite infill in coralline algae with phylomineralogy. The study contributes to the growing body of literature characterizing and speculating about how the relative abundances of carbonate biominerals in corallines may vary in response to changes in atmospheric pCO_2, ocean acidification, and global warming.

Key index words: **aragonite; calcite; coralline algae; Gulf of Mexico; Hapalidiales; ocean acidification; Panama; phylomineralogy; *psb*A; X-Ray microscopy**

***Abbreviations*: BS, bootstrap value; PP, posterior probability; SEM-EDS, Energy dispersive spectrometry; SEM, Scanning electron microscopy; XRD, X-ray diffraction**

All crustose coralline algae belonging in the Corallinales, Hapalidiales, and Sporolithales (Rhodophyta) are characterized by the presence of calcium carbonate in their cell walls, which is often in the form of highly soluble high-magnesium-calcite (Adey 1998, Knoll et al. 2012, Adey et al. 2013, Diaz-Pulido et al. 2014, Nelson et al. 2015). Besides the Rhodogorgonales (Fredericq and Norris 1995), a sister group of the coralline algae in the Corallinophycidae (Le Gall and Saunders 2007) whose members also precipitate calcite, all other calcified red and green macroalgae deposit calcium carbonate in the form of aragonite (reviewed in Adey 1998, Nelson 2009). Previous studies have also shown that the more stable carbonates, that is, aragonite and dolomite, may be present in the thallus of coralline algae filling in vegetative cells and pores (Alexandersson 1974, Nash et al. 2011, 2012, 2015). The pioneering study by Alexandersson (1974) using scanning electron microscopy (SEM), energy dispersive spectrometry (SEM-EDS), X-ray diffraction (XRD), and Feigl's solution staining to analyze the elemental and mineralogical condition of coralline-forming nodules known as rhodoliths, documented that empty reproductive conceptacles of *Lithothamnion glaciale* Kjellman rhodoliths from the Skagerrak in the North Sea become filled in with aragonite crystals, despite the undersaturated conditions of the local seawater favoring dissolution of calcium carbonate crystals. Subsequently, Walker and Moss (1984), using methods similar to Alexandersson (1974), showed that aragonite is precipitated in between the coralline crusts and their substratum, often when a space occurs between them. Unfortunately, since neither Alexandersson (1974) or Walker and Moss (1984) provided empirical SEM-EDS or XRD data in their studies, no comparisons can be made between their studies and newly generated data.

More recently, Smith et al. (2012) using XRD, reported the presence of aragonite in the mineral

[1]Received 1 June 2015. Accepted 18 December 2015.
2Author for correspondence: e-mail slk5014@louisiana.edu.
Editorial Responsibility: C. Hurd (Associate Editor)

composition of *Lithothamnion crispatum* Hauck, and Nash et al. (2011) and Diaz-Pulido et al. (2014) documented the presence of aragonite infill in cells of the reef-building coralline *Porolithon onkodes* (Heydrich) Foslie using EDS and XRD. Diaz-Pulido et al. (2014) also illustrated empty conceptacles of *P. onkodes* filled in with aragonite. Torrano-Silva et al. (2015) used micro-CT or 3D X-ray imaging on various coralline samples and concluded that the system could be applied to 3D models and that materials of different density could be individually analyzed. They stated that this tool would be applicable to the study of aragonite in coralline algae since it is very dense and can be distinguished from the other forms of calcium carbonate.

In the northern Gulf of Mexico, subtidal rhodolith beds harbor a diverse community of rhodolith-forming coralline algae (Felder et al. 2014, Fredericq et al. 2014, Richards et al. 2014) that have yet to be fully described and characterized. Preliminary SEM imaging of a biogenic rhodolith-forming coralline species identified on the basis of morphological and molecular evidence as belonging to the genus *Lithothamnion*, revealed aggregates of needle-like crystals present in their empty reproductive conceptacles. The specimens may conform to the species concept of *Lithothamnion occidentale* (Foslie) Foslie, described from Cruz Bay, St. John Island, US Virgin Islands, and reported for the Gulf of Mexico (Fredericq et al. 2009, Mateo-Cid et al. 2014). However, the type specimen of *L. occidentale* needs to be carefully examined before this species epithet can be assigned with confidence to the material examined. Likewise, a second species of *Lithothamnion* from the Gulf of Chiriquí, Pacific Panama, showed the same needle-like crystals in empty conceptacles. In typical light microscopy-based morphological and taxonomic treatments of corallines, hand-and microtome sections are made after decalcification of the thallus parts, hence removing all traces of the calcium carbonate mineralogy. In contrast, the present study did not decalcify the samples enabling the provision of empirical evidence to confirm the nature of the crystals in the complex internal structure and skeleton of the coralline rhodoliths, and to quantify their elemental composition with SEM-EDS, XRD, and ZEISS X-ray microscopy, which is a new state-of-the art, accurate and noninvasive tool (http://www.zeiss.com/microscopy/en_us/solutions/reference/x-raymicroscopy.html).

Biomineralization is an important and timely topic as the dynamic processes involved may be influenced by ocean acidification (Nelson 2009, Basso 2012). Smith et al. (2012) discussed the importance of providing empirical data in studies of biomineralization and noted that a fundamental problem in previous mineralogical studies is that results are often presented in a descriptive manner and lack quantitative data. Smith et al. (2012) also stressed the importance of analyzing mineralogical data in the context of phylogenetics, and utilized the molecular chloroplast marker *psb*A to establish a phylomineralogical framework. The present study answers the call by Smith et al. (2012) to provide empirical and quantitative data in the study of calcium carbonate biomineralization in corallines and to add *psb*A sequences in an expanding coralline *psb*A framework for phylomineralogy.

MATERIALS AND METHODS

Field collections. Specimens of the biogenic rhodolith-forming crustose coralline *Lithothamnion* sp. 1 and *Lithothamnion* sp. 3 were collected in the vicinity of the Florida Middle Grounds, 84° 02.7′ W, 28° 10.27′ N, between 43 and 42 m depth, on July 7, 2006 offshore in the NE Gulf of Mexico; and in the vicinity of Ewing Bank, 28° 05.845′ N; 91° 01.817′ W, between 54 and 58 m depth, on November 16, 2012 offshore in the NW Gulf of Mexico (Table 1) with an Hourglass-design box dredge using minimum tows (usually 10 min or less; Fredericq et al. 2014, Felder et al. 2014). A *Lithothamnion* sp. 2 specimen from the Gulf of Chiriquí, Pacific Panama, was collected by hand at a depth of 16 m while SCUBA diving (Table 1). Specimens were preserved in silica gel on site. Vouchers are deposited in the Algal Herbarium of the University of Louisiana at Lafayette (LAF).

Light microscopy. Specimens were examined under a Zeiss Stemi 2000-C stereomicroscope to remove all visible epiphytes. Habit protuberances were removed using a single-edged razor blade and forceps, and longitudinally hand-sectioned. No portions of the vouchers were decalcified. Photos of the habit were taken with a Canon PowerShot A3300 camera.

SEM. Five protuberances comprising five individuals each were selected for SEM, with each protuberance cut longitudinally into two approximately equal-sized pieces using a razor blade. The resulting sections were mounted using liquid graphite and coated with 11.5 nm of gold. SEM micrographs were produced using a Hitachi S-3000N SEM at a voltage of 15 kV. The SEM is housed in the Microscopy Center at UL Lafayette.

SEM-EDS. The same samples selected for SEM were used for SEM-EDS analyses using the Hitachi S-3000N and an IXRF system EDS 2000. One nonreproductive sample of *Lithothamnion* sp. 1 (LAF6521) was excluded from SEM-EDS measurements. To ensure accuracy in element concentration measurements, the input count rate was maintained at 1,000 c/s or higher. The working distance was between 15 and 25 mm and the voltage was at 25 kV. The live time for each measurement was 25–28 s. Element concentrations measuring less than 1% (by weight or mole %) were not included in the analyses. Individual crystals were quantified as often as possible. Five measurements were taken of vertical crystals located within conceptacles, and five measurements were taken of radial crystals located in the walls of cells that constitute the conceptacle walls. Two conceptacles were measured from each sample. Fast maps displaying element location and quantities were produced for each sample. A sample of pure aragonite (Ward's Geology Sales Catalogue 1998) was measured and used as a standard for comparison to the crystals measured in the rhodolith conceptacle. We hypothesized that the crystals found in the overgrown conceptacles would match the mole % of the aragonite standard.

X-ray diffraction. Three to four protuberances from each of the five specimens used for SEM and SEM-EDS were selected for XRD analysis. Protuberances that were already mounted as cross-sections for SEM and SEM-EDS were not

TABLE 1. Identification number, taxon, collection site, collector's name, and GenBank accession number for each studied specimen.

ID. no.	Taxa	Locality	Collector	GenBank accession no.	
				*psb*A	LSU
LAF1437A (LAF-7-5-06-2-2A)	*Lithothamnion* sp. 1	Florida Middle Grounds, 28° 10.27′ N; 84° 02.07′ W, 42–43 m	S. Fredericq 5.vii.2006	KP844863	KR075888
LAF1437B (LAF-7-5-06-2-2B)	*Lithothamnion* sp. 1	Florida Middle Grounds, 28° 10.27′ N; 84° 02.07′ W, 42–43 m	S. Fredericq 5.vii.2006	–	KR075889
LAF6521 (LAF 11-16-12-5-1)	*Lithothamnion* sp. 1	Ewing Bank, 28° 05.845′ N; 91° 01.817′ W, 54–58 m	J. L. Richards 16.xi.2012	KP844864	KR075890
PHYKOS7249 (LAF 5-11-13)	*Lithothamnion* sp. 2	Panama, 7° 28′ N; 81° 14′ W, 16 m	W. E. Schmidt 11.v.2013	KP844865	KR075891
LAF1437C (LAF-7-5-06-2-2C)	*Lithothamnion* sp. 3	Florida Middle Grounds, 28° 10.27′ N; 84° 02.07′ W, 42–43 m	S. Fredericq 5.vii.2006	–	KR075892

destroyed for XRD but preserved as vouchers (with the exception of the mounted protuberance of *Lithothamnion* sp. 1 sample LAF1437A, which was sacrificed and included in the material prepared for XRD). Protuberances were ground to a powder and the resulting material was transferred to a glass slide. The material on the slide was then analyzed using Phillips Automated XRD equipment. Data were collected at 40 kV and 25 mA of current. The two-theta scan was collected using a step size of 0.02 degrees angle for a 3-s collection interval. The samples were also spiked by fluorite (CaF_2) which acts as a standard and provides a more accurate measurement of the 2-theta angle for magnesium calcite. The theta value for magnesium calcite was in turn used to estimate the mol percent Mg in the Mg-calcite mineral using the cross plot published by Scholle (1978). Qualitative identification of the aragonite and Mg-calcite peaks was matched with reference standard peaks from the International Center for Diffraction Data (ICDD). The quantitative data were obtained using the Rietveld refinement method included in the MDI Jade 2010 software suite Materials Data Inc. Livermore, CA, USA.

Bruker SkyScan1176 microtomography (micro-CT). A single protuberance from rhodolith sample LAF1437A was sent to Bruker Corporation for analysis on the *SkyScan1176*. This equipment allows for high-definition scanning of objects using a cooled digital X-ray camera that is coupled by fiber optics to a scintillator (Bruker International Corporation). The analysis operated under a 68-mm field of view following the manufacturer's instructions.

ZEISS X-ray microscopy. The same rhodolith protuberance viewed with the *SkyScan1176* was sent to Zeiss for analysis on their ZEISS Xradia 520 Versa X-ray Microscope. 2D and 3D videos were generated using the "ORS Visual SI Advanced" software (Montreal, Quebec, Canada). Two scans were collected for the sample: the lower resolution scan was run with 3.42 μm and the higher resolution scan was run with 1.52-μm isotropic voxel resolution. Photoshop was used to capture one screen of the Z-plane from the 2D video provided by ZEISS (Video S1 in the Supporting Information). This figure was saved as a TIFF file, opened in ImageJ, and the total number of pixels were measured. The pixels of the dense (brighter) aragonite were then measured and a percentage calculated.

Molecular data acquisition. Total DNA was extracted from silica gel-dried specimens using a DNeasy Plant Mini Kit (Qiagen, Valencia, CA, USA) following the manufacturer's instructions. The DNA was extracted from the same specimens used for the SEM, SEM-EDS, and XRD analyses to confirm the correct identity of the corallines. Voucher specimens are deposited at LAF. The chloroplast-encoded gene *psb*A was selected for PCR using the primers referenced in Yoon et al. (2002) and protocols referenced in Richards et al. (2014). Resulting PCR products were sequenced in-house on an ABI Model 3130xl Genetic Analyzer. Because *psb*A was successfully amplified for only three of the five specimens in this study, a portion of the nuclear-encoded LSU rDNA was also amplified and sequenced using the primers and PCR protocol referenced in Sherwood et al. (2010) to generate reference barcodes for each of the five specimens. The sequences were uploaded to GenBank (Table 1) to provide reference markers for future phylomineralogical studies.

Alignment and phylogenetic and barcoding analyses. A *psb*A alignment was constructed using the sequences used by Smith et al. (2012) (see Table 1 and Table S1 in the Supporting Information for list of sequences analyzed in this study) to establish the phylomineralogical framework for corallines with the addition of the *Lithothamnion* sp. 1 and sp. 2 sequences generated in this study. The alignment was 863 bp in length and analyzed in Partition Finder (Lanfear et al. 2012) to determine the best partition scheme and model(s) of evolution as can be implemented by RAxML. A three-codon position partitioning scheme, each evolving with GTR+I+ G model was selected on the basis of the Akaike information criterion, corrected Akaike information criterion, and Bayesian information criterion. The alignment with the above models and partitioning scheme was then analyzed for Maximum Likelihood (ML) with RAxML v 2.4.4 (Stamatakis 2006) and 1,000 bootstrap replicates in order to assess branch support. Bayesian analysis was performed on the alignment using Mr. Bayes 3.2.5 (Ronquist et al. 2012). Two parallel analyses were conducted, each consisting of four MCMC chains (three heated and one cool) with 2.5×10^6 generations. Resampling was performed every 1,000 generations resulting in a total of 5,002 trees for both runs. The first 10% of each run was discarded as "burn-in," and a consensus tree was built with remaining data. Convergence was determined with Tracer v1.6 (Rambaut et al. 2014) An LSU alignment was constructed using sequences generated in this study and sequences downloaded from GenBank (Table 1 and Table S1). Sequences were initially aligned in MacClade 4.08 (Maddison and Maddison 2000) then exported and aligned using the CLUSTAL W (Thompson et al. 1994) program in MEGA 5.2.2 (Tamura et al. 2011). Ambiguous regions in the LSU alignment were cropped to the nearest conserved region and the alignment was truncated to correspond to the size of the amplicon (~600 bp before cropping ambiguous regions) generated by the primers referenced in Sherwood et al. (2010). The final alignment (Fig. S1 in the Supporting Information) was 431 bp in length and was analyzed for distance using the neighbor-joining (NJ) program in MEGA 5.2.2 (Tamura et al. 2011) with the maximum composite likeli-

hood model and 2,000 bootstrap replicates in order to assess branch support. Because this marker was used primarily as a barcode and is relatively short and conserved, ML and Bayesian analyses were not conducted.

RESULTS

SEM. Longitudinal sections of protuberances (Fig. 1A) show flared epithallial cells (Fig. 1B) and reveal the presence of multiple overgrown conceptacles within the protuberances of *Lithothamnion* sp. (Fig. 1C). Many of these conceptacles are filled with needle- or dagger-like vertical crystals (Fig. 1D). These conceptacles are overgrown by new vegetative filaments arising from the perithallial filaments surrounding the conceptacles (Fig. 1, D and E). Perithallial filaments arch over the conceptacle roof where they assume a hypothallial morphology by growing over the old conceptacle roof which now functions as the new substratum. From the newly formed hypothallus, arching tiers of perithallial filaments curve away in a direction perpendicular to the conceptacle roof. The result of this development leads to protuberances with a skeletal structure that is largely formed from layers of old conceptacles, with each overlapped layer of new vegetative growth subsequently giving rise to the next conceptacle(s). The conceptacles at the base of the protuberance are the oldest and the conceptacles near the tip the youngest (Fig. 1C). In addition to the presence of vertical crystals in the conceptacle lumen, radial crystals (Fig. 1, E and F) are shown in walls of conceptacle cells.

SEM-EDS. Fast maps (Fig. 2, A–D) of elemental composition detected with EDS focused on the boundaries inside and outside of the conceptacle shown in Figure 1D. The fast maps revealed the presence of calcium (Fig. 2B), carbon (Fig. 2C) and oxygen (Fig. 2D) in the radial crystals located in the walls of the vegetative cells surrounding the conceptacle, as well as in the putative aragonite crystals within the conceptacles, indicating the presence of calcium carbonate. The presence of magnesium (Fig. 2A) was detected in the crystals in the vegetative cell walls but not in the putative aragonite crystals within the conceptacles. The elemental composition of radial crystals in the walls of cells from the conceptacle wall (Fig. 1, A and F) showed the presence of Ca, C, Mg, and O, whereas the elemental composition of the vertical crystals within

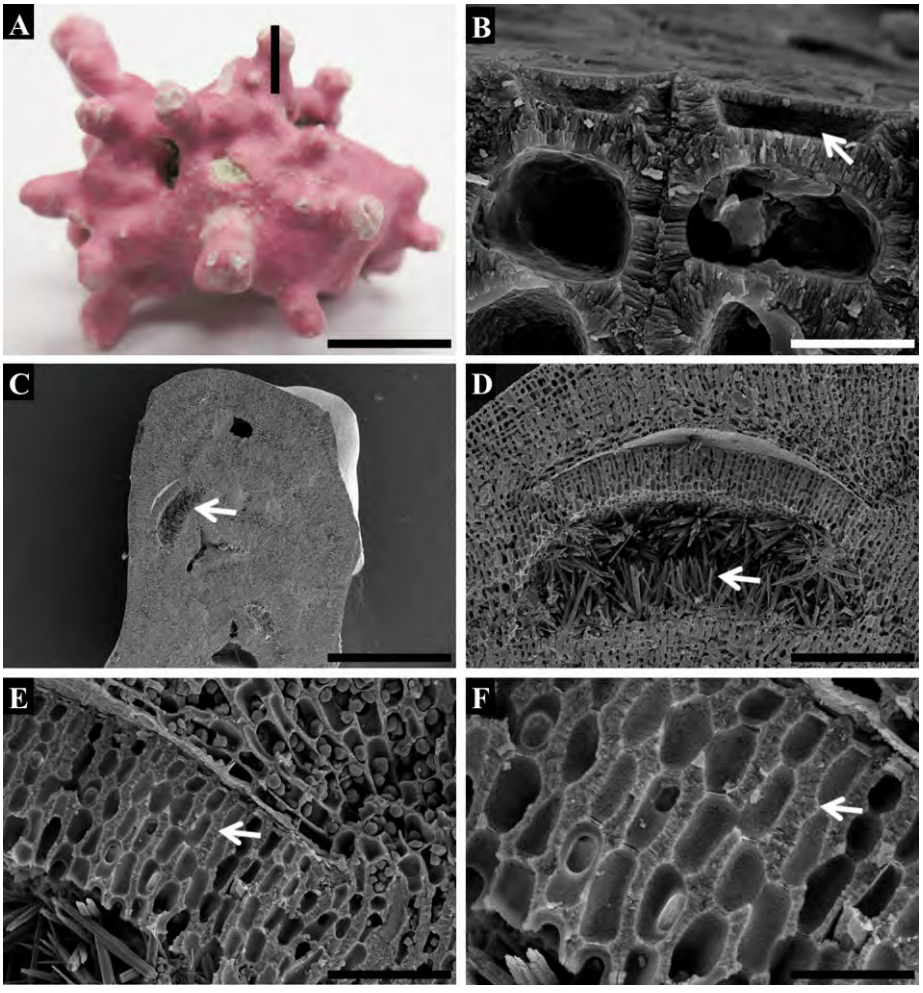

FIG. 1. *Lithothamnion* sp. 1 (LAF1437A) rhodolith from the vicinity of the Florida Middle Grounds, FL. (A) Habit and protuberances (longitudinalstripe) that house the conceptacles; (B) Epithallial cells (arrow) with flared corners; (C) Longitudinal section through protuberance from specimen shown in (A) displaying overgrown empty conceptacles and those filled in with aragonite crystals (arrow); (D) Detail of overgrown conceptacle shown in C filled with dagger-shaped, vertical aragonite crystals (arrow); (E) Perithallial filaments (upper right) growing over the conceptacle roof, and detail of aragonite crystals (lower left). Radial crystals composed of magnesium-rich calcium carbonate (arrow); (F) Magnified view of (E) showing horizontal magnesium-rich calcium carbonate crystals in walls of conceptacle cells. Scale bars: 4mm for A, 7 μm for B, 1.2 mm for C, 225 μm for D, 60 μm for E, and 25 μm for F.

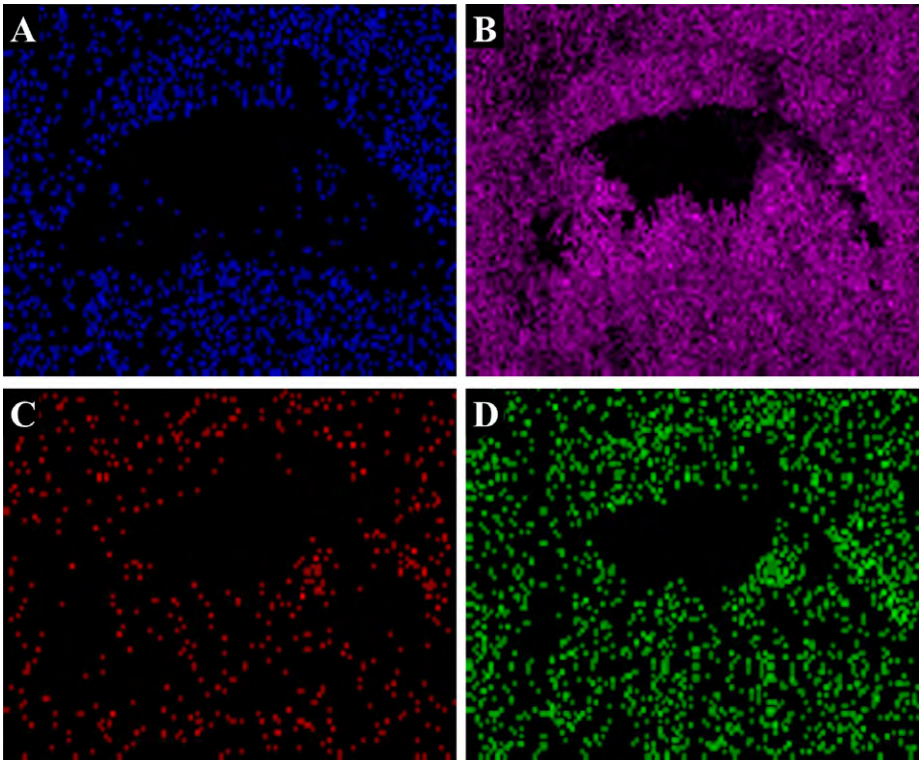

FIG. 2. *Lithothamnion* sp. 1 (LAF1437A) rhodolith from the vicinity of the Florida Middle Grounds, FL. Fast maps of elemental composition detected with EDS focused on the inside and outside of conceptacle shown in Fig. 1D); (A) Magnesium; (B) calcium; (C) carbon; (D) oxygen. Note the relative absence of Mg in location of aragonite crystal fill-in inside conceptacle.

the conceptacles (Fig. 1D) included only Ca, C, and O. Overall trends of element concentration were noted in all of the samples measured (Fig. 3). The SEM-EDS graph shows the average of five random measurements from two conceptacles of each sample, with individual columns representing the % mol of elements found in vertical crystals located inside conceptacles or radial crystals located within conceptacle walls. Two measurements were taken from *Lithothamnion* sp. 1 (LAF1437A-B), one from *Lithothamnion* sp. 3 (LAF1437C) (NE Gulf of Mexico), and one from *Lithothamnion* sp. 2 (PHYKOS7249) from Pacific Panama. The average amount of calcium present in the radial crystals from the cells of the conceptacle wall (44.13% mol) was less than the amount measured in crystals located within the conceptacles (51.33% mol) and significantly different, *P*-value = 0.00202 (degree of 13.809, *t*-value = 3.792; Fig. 3). The Welch two sample *t*-test was completed using R version 3.2.2 (Welch 1947, Team 2010). It compared the average concentration of calcium, magnesium, carbon, and oxygen between the samples and a controlled standard from Ward's ($t = 0.197$). To test our EDS equipment we collected data on a standard of aragonite. The aragonite standards were determined to be 49.91% mol Ca, 37.27% mol O, 3.09% mol C, and 0% mol Mg. The amount of Ca in the aragonite standard (Ward's) is reported as 49.91% mol, which is statistically identical to the elemental concentrations we found in the crystals shown in Figure 1C. Carbon and oxygen concentrations were similar in the vegetative cells of the conceptacles and in the aragonite crystals from within conceptacles (Fig. 1C). Magnesium was not detected inside (0% mol) the conceptacles but showed an average concentration of 5.04 mol% $MgCO_3$ in the conceptacle wall (*P*-value = 1.63×10^{-6}, $t_7 = -14.68$; corresponding to Fig. 1D).

X-ray diffraction. Qualitative and quantitative identification of aragonite and Mg-calcite peaks were assessed against reference standard peaks from the ICDD. The quantitative data were obtained by utilizing Rietveld refinement including the MDI Jade 2010 software suite, which indicates that the amount of aragonite varies in samples collected at three general locations, that is, *Lithothamnion* sp. 1 from Ewing Bank, NW Gulf of Mexico and the vicinity of the Florida Middle Grounds, and *Lithothamnion* sp. 2 from the Gulf of Chiriqui, Pacific Panama. The aragonite amount varies from 0% at Ewing Bank to 9.4% in Pacific Panama (Fig. 4). The XRD data of samples spiked by fluorite (CaF2) is presented in Figure 5. The estimated mol % Mg in the Mg-calcite mineral is noted in the graphs for each sample. For example, the sample from Ewing Bank, which has no detectable amounts of aragonite, contains 21 mol % Mg, while the sample from Pacific Panama, which contains 9.4% aragonite, represents 22 mol % Mg in the magnesium calcite structure. The aragonite needles emerging beyond the walls of the conceptacles make up a very small fraction of the thallus; therefore, the peaks detected by XRD for aragonite are small. Despite the small peaks, the

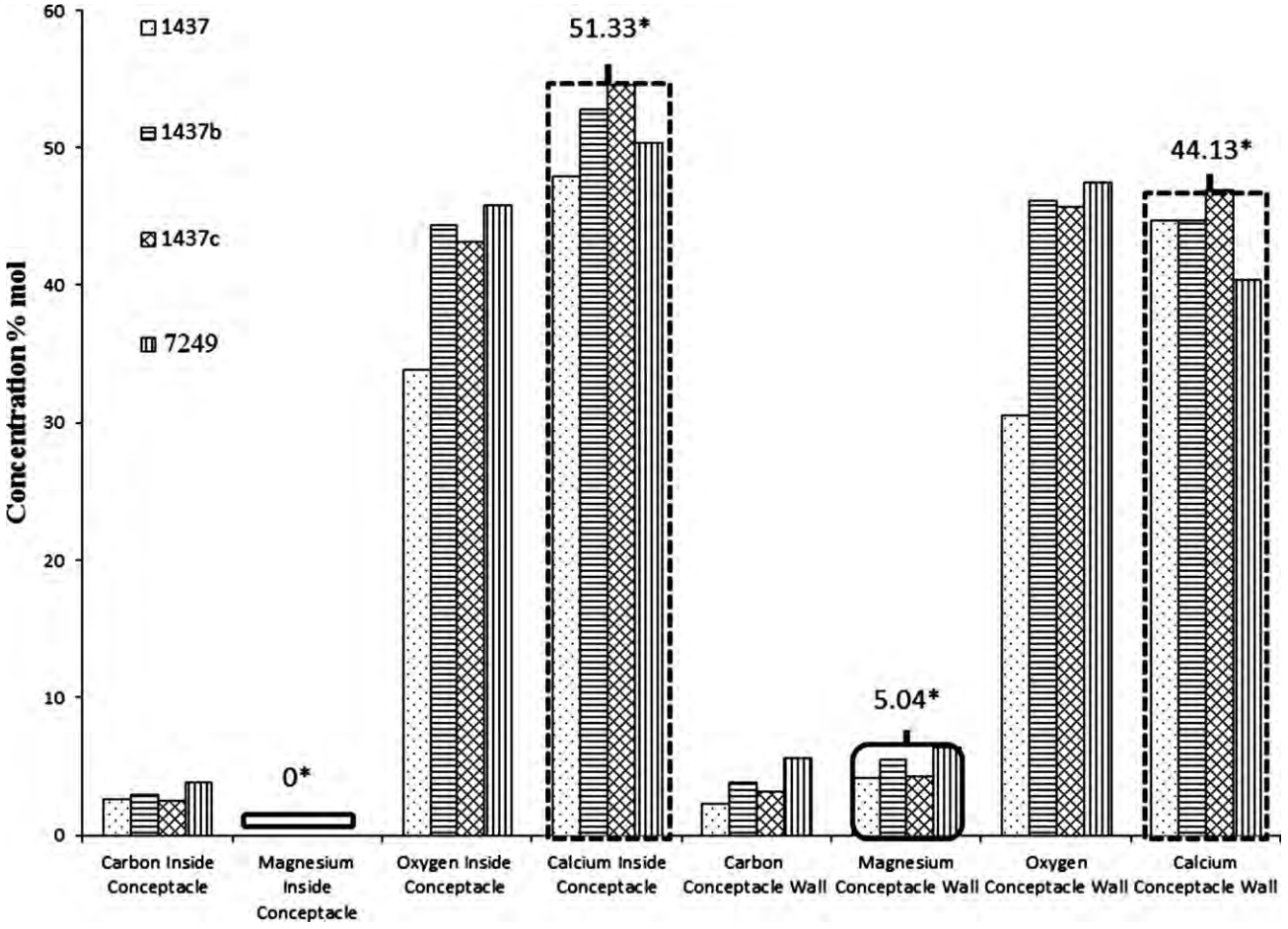

FIG. 3. SEM-EDS graph showing average of five random measurements from two conceptacles of each sample: two measurements from *Lithothamnion* sp. 1 (LAF1437A-B), one measurement from *Lithothamnion* sp. 3 (LAF1437C) from the Gulf of Mexico, and one measurement from *Lithothamnion* sp. 2 from Pacific Panama (PHYKOS7249). Individual columns represent the % mol of elements found in vertical crystals located inside conceptacles (Fig. 1D, arrow), or radial crystals located within conceptacle walls (Fig. 1E, arrow and F). Solid boxes = % mol Mg, dashed boxes = % mol Ca, * = statistical difference between crystals found inside conceptacles or crystals found in cells forming the conceptacle wall. Values posted are average % mol concentrations of all samples measured for a specific element.

aragonite has been positively identified by XRD (Figs. 4 and 5) in all reproductive samples analyzed (data from sample LAF1437A is not shown here and is available from the authors by request). In contrast, no aragonite was detected in the nonreproductive sample (LAF6521) from Ewing Bank.

Bruker SkyScan1176 microtomography (micro-CT). A still image (Fig. 6A) of the vegetative cells and filaments, conceptacles, and aragonite infill in sample LAF1437A was captured from a 2D-video.

X-ray microscopy. ZEISS X-ray microscopy shows still images (Fig. 6, B and C) of the vegetative cells and filaments, conceptacles, and aragonite infill in sample LAF1437A captured from 2D and 3D videos produced (Video S1). This tool allows aragonite, a dense form of calcium carbonate, to be visualized and quantified. Using ImageJ (Rasband 1997-2014), the percentage of aragonite in one Z-plane of sample LAF1437A was calculated to be 5.446%.

Phylogenetic and barcoding analyses. The ML (Fig. S2 in the Supporting Information) and Bayesian analyses (Fig. 7) resulted in identical topologies, for nearly all clades, with differences only in the branching order of the clade comprised of *Mesophyllum engelhartii* and *M. macroblastum.* In the ML analyses this clade is nested within the other Hapalidiaceae species comprising a branch with low support (BS 53%) that is sister to the clade comprised of *Phymatolithon repandum*, *Mesophyllum erubescens*, and *M. printzianum.* In the Bayesian analyses *M. engelhartii* and *M. macroblastum* comprise a clade that is sister to the other Hapalidiaceae species with strong support (PP 0.95). Support values were overall higher in the Bayesian analyses than in the ML

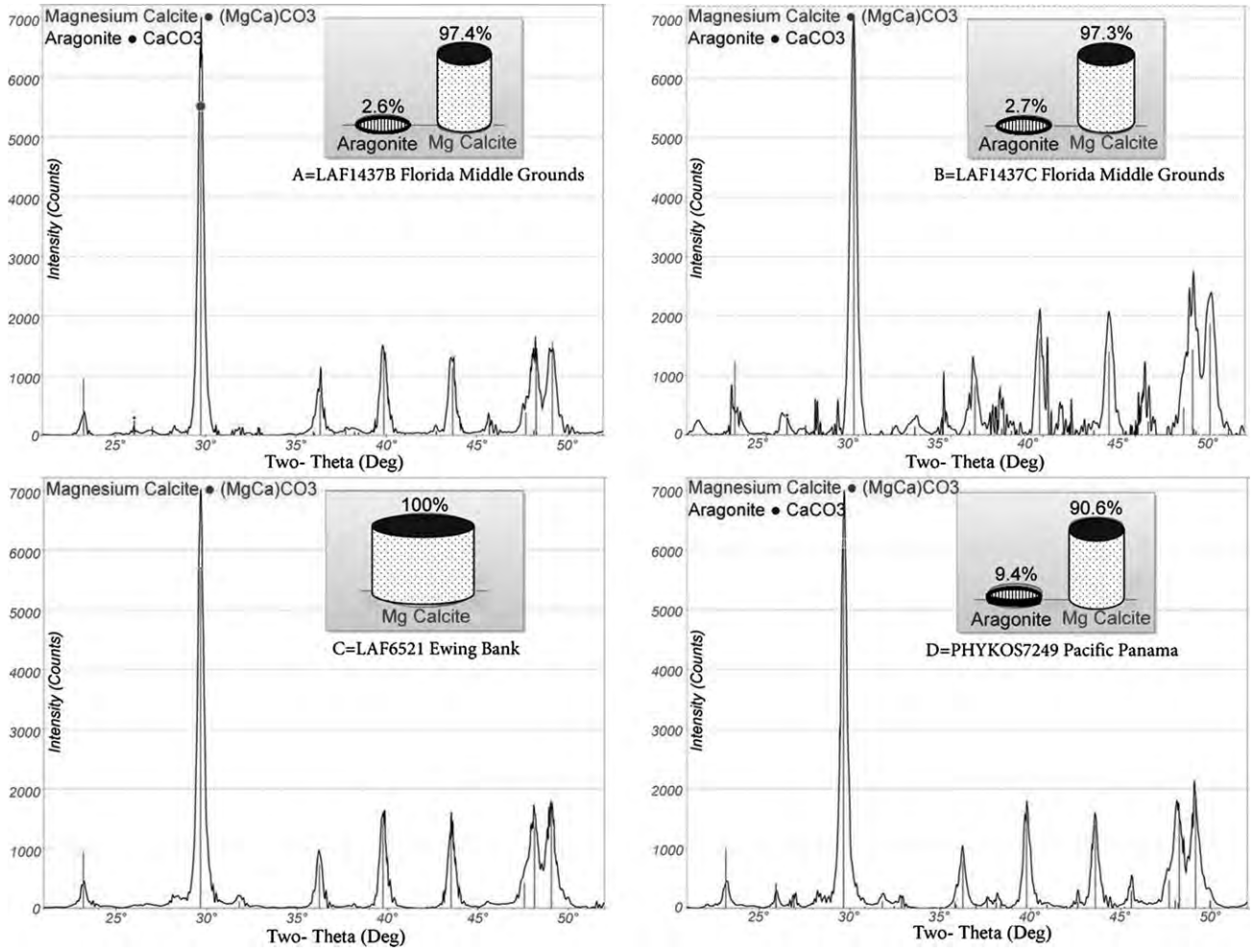

FIG. 4. Qualitative & quantitative identification of aragonite and Mg-calcite peaks with reference standard peaks accessed from the International Center for Diffraction Data (ICDD). Quantitative data were obtained by utilizing Rietveld refinement including the MDI Jade 2010 software suite, which indicates that the amount of aragonite at the four locations varies from 0% at Ewing Bank to 9.4% in Pacific Panama. (A, B) samples from Florida Middle Grounds, NE Gulf of Mexico; (C) Ewing bank, NW Gulf of Mexico; (D) Gulf of Chiriquí, Pacific Panama. Lack of conceptacles in (C); the presence of conceptacles in A, B and D.

analyses. *Psb*A sequences of *Lithothamnion* sp. 1 from the northern Gulf and of *Lithothamnion* sp. 2 from Pacific Panama resulted in phylogenetic ML trees in which the two taxa were sister to each other with strong (BS 97%, PP 1) support (Figs. 7 and S2). The two *psb*A sequences of *Lithothamnion* sp. 1 were identical to each other and differed from the sequence of *Lithothamnion* sp. 2 by 21 bp (2.4%). This cluster of *Lithothamnion* sp. 1 and sp. 2 sequences was sister to the published sequence of *L. crispatum* with moderately strong (BS 87%) support in the ML analyses but with full support in the Bayesian analyses (BS 87%, PP 1).

The results of the NJ LSU analysis (Fig. S3 in the Supporting Information) indicate that specimens of *Lithothamnion* in this study represent three distinct species (*Lithothamnion* sp. 1, sp. 2, and sp. 3) in two separate clusters within the Hapalidiaceae. The LSU sequences of samples LAF1437A and LAF1437B were identical to each other indicating they likely represent the same taxon (*Lithothamnion* sp. 1). *Lithothamnion* sp. 1 and sp. 2 comprise a clade with full support with a topology identical to the *psb*A tree. LSU sequences of specimens of *Lithothamnion* sp. 1 differed from each other by 0–1 bp (0%–0.2%) and differed from the sequence of *Lithothamnion* sp. 2 by 3–5 bp (0.7%–1.2%). The LSU sequence of *Lithothamnion* sp. 3 comprise a clade separate from *Lithothamnion* sp. 1 and sp. 2, sister to a specimen identified as Unidentified Hapalidiaceae (GQ917333) from New Caledonia with moderate low support (BS 63%), and differed from *Lithothamnion* sp. 1 and sp. 2 by 14–15 bp (3.2%–3.5%).

DISCUSSION

The presence of magnesium in the radial crystals of the vegetative cells, coupled with a relative

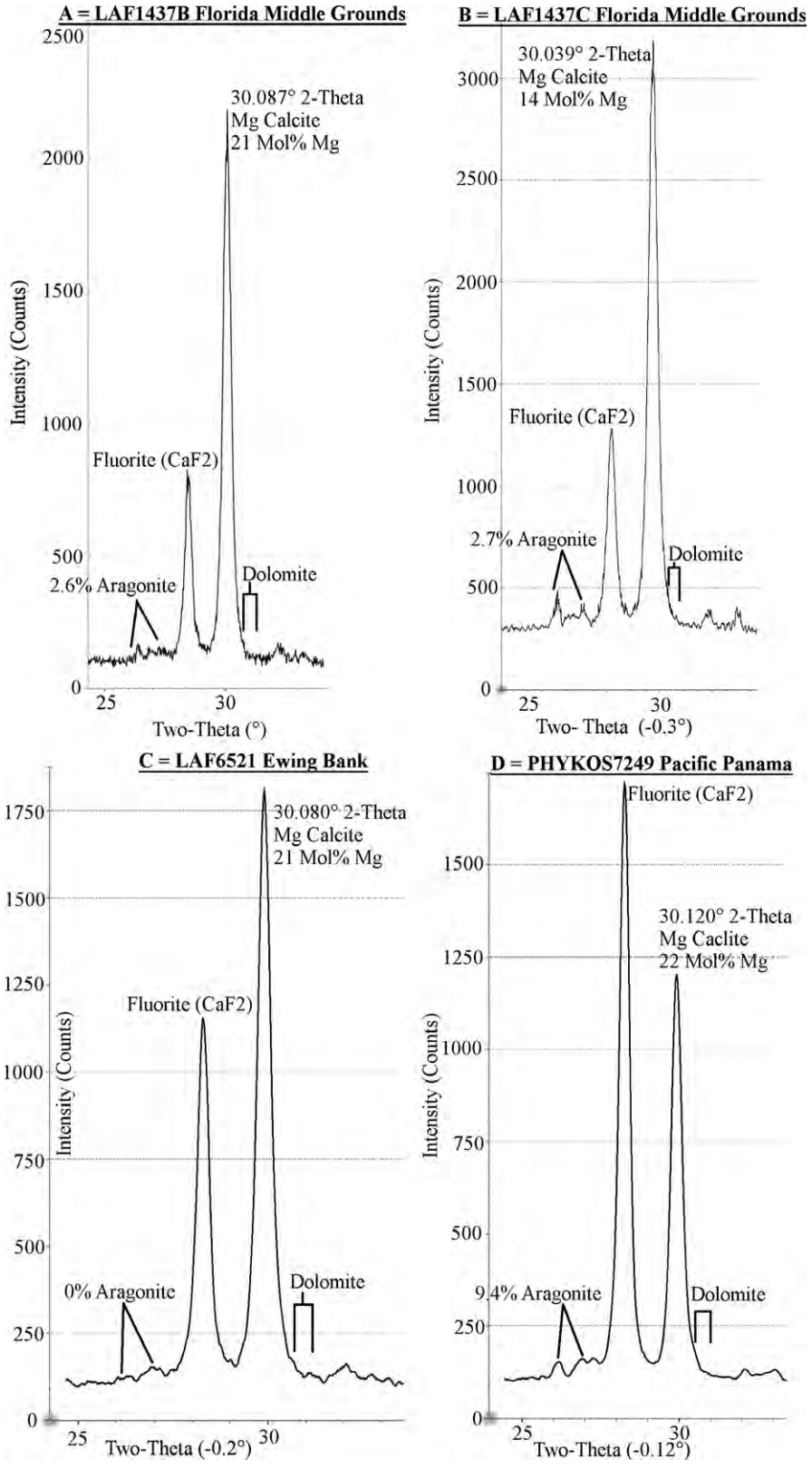

FIG. 5. XRD data of *Lithothamnion* samples spiked by fluorite (CaF_2) to obtain a more accurate measurement of the 2-theta angle for magnesium calcite. The theta value for magnesium calcite was used to estimate the mol % Mg in the Mg-calcite mineral, noted in the graphs for each sample. (A, B) Florida Middle Grounds; (C) Ewing Bank; (D) Pacific Panama. Lack of conceptacles in (C); presence of conceptacles in (A, B and D).

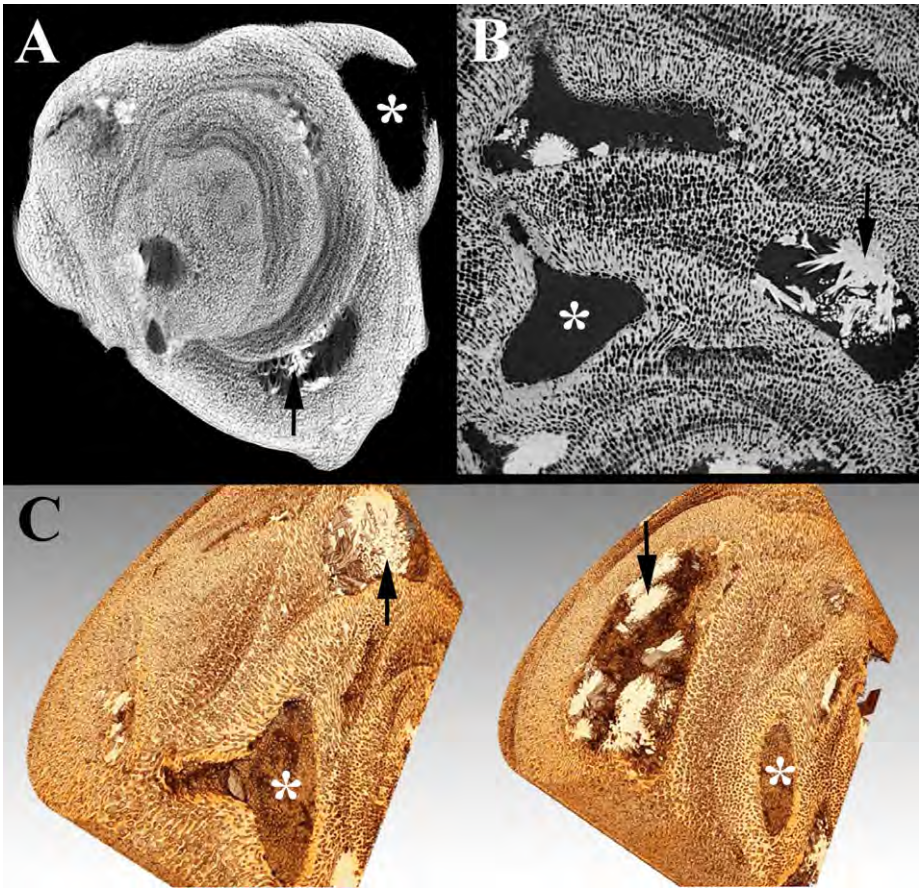

FIG. 6. (A–C) *Lithothamnion* sp. protuberance of rhodolith sample LAF1437A, * denotes conceptacle, arrow denotes aragonite infill. (A) Bruker Microtomography image (μ-CT), (B, C) ZEISS Xradia 520 Versa' X-ray Microscope images generated from 2D-video (B) and 3D-video (C) videos using "ORS Visual SI Advanced" software. (A) Vegetative filaments, conceptacles and aragonite infill. (B) Detail of sample shown in C, scale bar = 100 μm. (C) Two different in situ focal planes of same protuberance captured showing various depths of vegetative filaments, conceptacles, and aragonite infill. Scale bars in A and C were not provided by Zeiss or Bruker.

absence of magnesium in vertical crystals within the conceptacle, indicates that the vegetative cell crystals are composed of high-magnesium calcite and that the crystals within the empty conceptacles are comprised of aragonite. The shape of the vertical crystals shown in the illustrated empty conceptaces are identical to those referenced by Alexandersson (1974) (p. 17, fig. 7). The presence of aragonite in the senesced conceptacles of *Lithothamnion* begs the question, "what causes these crystals to nucleate and grow"? Alexandersson (1974) proposed that the living surface layer of rhodoliths from the Skagerrak formed a protective layer that created an internal microenvironment favorable for carbonate precipitation; however, he noted that identifying the mechanisms for internal rhodolith cementation (i.e., mineral infill) was beyond the scope of his study.

Adey (1998, p. 394) reviewed four key conditions under which biomineralization occurs in marine macroalgae, including: (i) enclosure within cells or tissue, (ii) presence of organic molecules for crystal initiation sites, (iii) active transport of necessary ions, and (iv) an organic matrix to organize crystal shape and texture. As is the case in *Halimeda*, a calcifying siphonous green seaweed (Ulvophyceae), only the first two conditions occur; as a consequence, calcification is in the form of disorganized aragonite crystals. Like in *Halimeda*, only the first two conditions occur in overgrown conceptacles of *Lithothamnion*. It can be speculated that condition 3 would not exist inside the conceptacles or the dynamics of active transport would be altered. The cells composing the conceptacle chamber wall would likely transport ions differently than do individual cells within the conceptacle, which can fill with crystals. Ion transport may also change upon reproduction, relative to the timing of sporogenesis or gametogenesis. Condition 4 is absent in the conceptacles of *Lithothamnion*; the organic matrix, normally found in the cell walls of coralline vegetative cells, is not present in the conceptacle lumen.

Walker and Moss (1984) investigated crustose coralline algal attachment methods as they relate to mineralization. In their study, it was observed that upon formation of a space in between the attached crust and the substratum, aragonite crystals were precipitated below the crust and filled in the space helping in crust reattachment. Walker and Moss (1984) proposed that metabolites secreted by the hypothallial cells may play a role in influencing aragonite precipitation. Woelkerling (1988), using light microscopy, provided evidence that after spores and gametes are released from the conceptacle, adventitiously formed vegetative cells fill in the

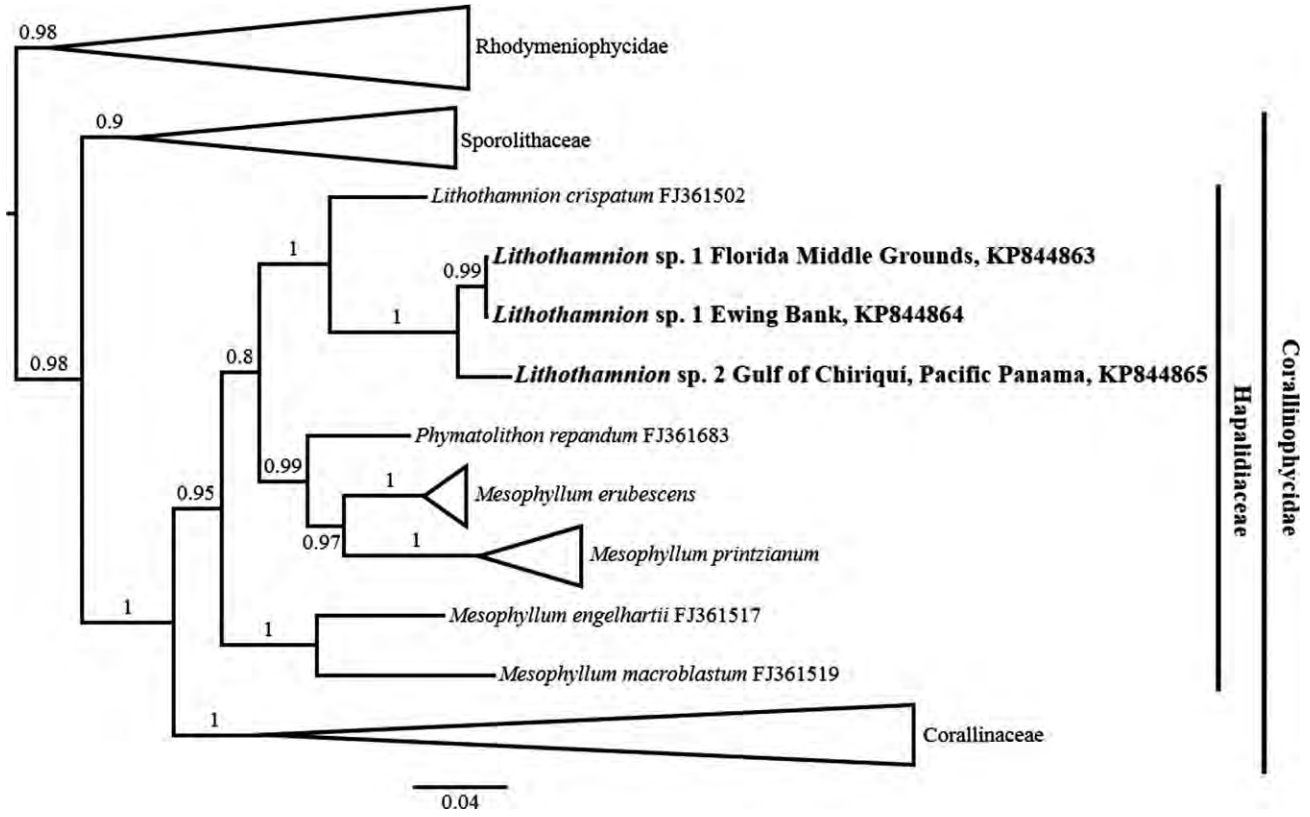

FIG. 7. Phylogram showing position of newly generated sequences (shown in bold) of *Lithothamnion* sp. 1 and sp. 2 in the Hapalidiaceae inferred from Bayesian analyses of *psb*A sequences. Numbers above branches indicate Bayesian posterior probabilities. Scale bar indicates number of substitutions per site.

conceptacle void in some genera. While it is intriguing to speculate that in some taxa these adventitious cells may provide metabolites that are involved in crystallization, Woelkerling (1988) did not document or report the presence or absence of aragonite crystals, which, had they been present, would have been lost to decalcification during slide preparation. The SEM micrographs taken during this study did not display adventitious cells in the conceptacles. We propose that metabolites released by vegetative cells composing the conceptacle wall could influence the seawater chemistry and microenvironment within the conceptacles, favoring aragonite precipitation.

De Choudens-Sánchez and González (2009) showed that in an experimental abiotic system, aragonite precipitation is favored over calcite precipitation when there is a high Mg/Ca ratio and low supersaturation levels of Mg and Ca. Perhaps metabolites released into the empty conceptacles raise the Mg/Ca ratio influencing the precipitation of aragonite. It can also be speculated that the larger space of the conceptacle void relative to the space of the individual cells and their interwall and intermembrane spaces may result in lower supersaturation levels of Mg and Ca ions in the conceptacle void (i.e., active transport of ions in the small spaces of vegetative cells may be high enough to raise supersaturation to favor Mg-calcite precipitation in cell walls, while active transport of ions into the larger conceptacle void does not raise the supersaturation levels enough to influence the precipitation of Mg-calcite in the empty conceptacle). Previous studies (reviewed in De Choudens-Sánchez and González 2009) have shown that Mg ions may also hinder calcite nucleation in solutions with low supersaturation levels. Perhaps the presence of Mg ions coupled with the speculated low supersaturation levels may also hinder the nucleation of calcite crystals within the empty conceptacles. Furthermore, if metabolite production is not causing the growth of these aragonite crystals, perhaps instantaneous precipitation is made possible by the physical protection of the conceptacle roof, that is, the conceptacle roof may provide protection from the abrasion on the free-living rhodoliths caused by wave action that may otherwise scour away the spontaneously precipitated crystals.

Bressan et al. (2007) proposed that Bruker microtomography might optimize the investigation of rhodoliths besides SEM. We go one step further and propose that Zeiss Xradia 520 Versa' X-ray microscopy might also be an excellent nondestructive tool to view in 3D context the exact location,

timing and degree of calcium carbonate polymorph infill concomitant with that of the development of algal filaments and reproductive structures within rhodoliths. This virtual X-ray microscopy sectioning in 3D, in addition to the 2D virtual sectioning provided by microtomography, may greatly enhance our future ability to quantify aragonite volume infill. Used in combination with ImageJ (Rasband 1997-2014), the percent aragonite can be readily calculated. While we only calculated the percent of aragonite in a single Z-plane to show the application of X-ray microscopy to rhodolith calcification patterns, this tool is capable of calculating the entire %/per volume within a particular structure which will greatly expand the ability to quantify and unambiguously locate aragonite in situ within rhodoliths.

Moberly (1970, 1973) noted that aragonite precipitation can occur rather quickly after conceptacles become overgrown. The results of our study support this hypothesis, as conceptacles with aragonite infill were found near the surface of the protuberance, indicating that aragonite in-fill may have occurred within a time frame as short as two reproductive cycles. Nash et al. (2011) reported that some conceptacles of *P. onkodes* (Heydrich) Foslie (as *Hydrolithon onkodes* [*Heydrich*] Penrose & Woelkerling) were filled in with dolomite and magnesite. This is not the case in the *Lithothamnion* spp. specimens observed in our study. The mineralogy of conceptacle in-fill in other coralline taxa needs to be confirmed by empirical studies to ascertain whether the presence of dolomite and magnesite in conceptacles are environmentally induced or physiologically induced by the cells of the corallines. Physiological induction of mineralization would be phylogenetically important in the characterization of certain clades of coralline algae. Despite the small sample size investigated in this study, it is intriguing that the only nonreproductive sample (LAF6521) was also the only sample that showed an absence of aragonite in the XRD analysis, a phenomenon that warrants additional research.

Previously, several authors (reviewed in Nelson 2009, Basso 2012) have reported that coralline algae, with their high Mg-calcite skeleton, may be more vulnerable to dissolution in response to increasing ocean acidification as compared to other marine calcifying organisms that precipitate aragonite. However, the findings in our study indicate that a portion of the skeletal mineral content of the Gulf of Mexico *Lithothamnion* rhodoliths can be composed of aragonite. This may alter the dynamics of dissolution in these particular rhodoliths, as compared to rhodoliths containing primarily a high Mg-calcite calcium carbonate skeleton. Aragonite is more abundant in older conceptacles, a trend we observed that is compatible with Moberly's (1973) and Alexandersson's (1972) observations that aragonite may commonly replace Mg-calcite. The results of the present study confirm earlier observations by Alexandersson (1974) and Smith et al. (2012) that coralline skeletal remains of *Lithothamnion* may also provide a larger fraction of aragonite to sediments than those of other nongeniculate coralline algal taxa. More research needs to be done to ascertain whether the aragonite infill in empty conceptacles is closely linked with hypothallial filament overgrowth of the conceptacle in other coralline taxa besides *Lithothamnion* (as well as other species of *Lithothamnion*, such as *L. crispatum*) and whether these data are phylogenetically informative at the ordinal level, since the Hapalidiaceae, the family to which *Lithothamnion* belongs, was recently elevated to ordinal level, the Hapalidiales (Nelson et al. 2015). No such distinct hypothallial overgrowth has been reported so far in *Porolithon* Heydrich—the widely used study organism for biomineralization studies—or in Corallinales as a whole. The protuberance growth pattern shown here for *Lithothamnion* spp., which is similar for several additional rhodolith-forming Hapalidiales taxa from the Gulf of Mexico (Richards, unpubl. data) differs from that reported for Corallinales taxa worldwide where protuberances are formed primarily from nonhypothallial overgrowth (see e.g., Woelkerling 1988, figs. 193–196).

The results of the ML and Bayesian analyses were congruent with the *psb*A analyses published in Smith et al. (2012) with respect to topology and branch support. The high similarity of *psb*A sequences of *Lithothamnion* sp. 1 (100%) and of LSU sequences of *Lithothamnion* sp. 1 (99.8%–100%) provides evidence that these three investigated specimens from the northern Gulf of Mexico are conspecific. *Psb*A sequence divergence values between *Lithothamnion* sp. 1 and *Lithothamnion* sp. 2 (2.4%) indicate that these specimens likely represent different species (see Pardo et al. 2014 and for more information regarding *psb*A divergence values and hypotheses of species boundaries). Interspecific variation between *Lithothamnion* sp. 1 and sp. 2 was relatively lower for LSU (0.7%–1.2%); however, this marker is relatively conserved in other clades of coralline algae (Richards et al. 2014), and thus these values are not in contrast with our species concept hypotheses. *Psb*A was not successfully amplified for *Lithothamnion* sp. 3, and thus its phylogenetic placement in the *psb*A phylogeny could not be determined. However, LSU sequence dissimilarity between this specimen and *Lithothamnion* sp. 1 and sp. 2 (3.2%–3.5%) was much higher than the interspecific variation between *Lithothamnion* sp. 1 and sp. 2, indicating that this specimen represents a different species. Further phylogenetic comparisons were beyond the scope of this study. Specimens referred to here as *M. erubescens* (Fig. S2, Fig. 7) and included in Smith et al. (2012), were recently shown with molecular data to comprise a clade separate from the clade that includes the holotype of *M. erubescens* (Foslie) Lemoine by Sissini et al. (2014) and Nelson et al. (2015) noted that these specimens likely represent

multiple species. However, in this study we have chosen to use the name published in Smith et al. (2012).

This is the first report on the presence of aragonite crystals in *Lithothamnion* rhodolith spp. in the Gulf of Mexico and Pacific Panama, and the first study to rigorously link SEM, SEM-EDS, and XRD data of aragonite infill in coralline algae with phylomineralogy.

We thank the National Science Foundation (DEB-0315995, DEB-1027110) for pre-Deepwater Horizon oil spill biodiversity research in the Gulf of Mexico. This research was also made possible in part by a Coastal Water Consortium of the The Gulf of Mexico Research Initiative (GoMRI-I), and GoMRI-III, following the 2010 Macondo oil spill. We also thank NSF grant DEB-1455569 for research on rhodoliths from Panama. We thank William E. Schmidt, Darryl Felder, and Nancy Rabalais for their support and interest, and the crew of the R/V *Pelican*, especially Alex Ren, for their help with sampling protocols aboard ship. We thank present and former members of the UL Lafayette Seaweeds Lab for help with sampling protocols. We greatly acknowledge Tom Pesacreta and Mike Purpurea at the UL Lafayette Microscopy Center for help and advice while using the SEM and EDS. We thank Bruker Corporation for imaging a sample on the SkyScan1178 Microtomography, Rachna Parwani and Carl Zeiss X-ray Microscopy for imaging the samples on the ZEISS Xradia 520 Versa' X-ray Microscope, Ian Usie for enhancing our XRD graphs, and Scott Duke-Sylvester for help with statistics. William E. Schmidt and two anonymous reviewers are thanked for their valuable comments on the manuscript.

Adey, W. H. 1998. Coral reefs: algal structured and mediated ecosystems in shallow, turbulent, alkaline waters. *J. Phycol.* 34:393–406.

Adey, W. H., Halfar, J. & Williams, B. 2013. The coralline genus *Clathromorphum* Foslie emend Adey; biological, physiological and ecological factors controlling carbonate production in an Arctic/Subarctic climate archive. *SI Contr. Mar. Sc.* 40:1–41.

Alexandersson, T. 1972. Intragranular growth of marine aragonite and Mg-calcite: Evidence of precipitation from supersaturated sea water. *J. Sediment. Petrol.* 42:441–460.

Alexandersson, T. 1974. Carbonate cementation in coralline algal nodules in the Skagerrak, North Sea; biochemical precipitation in undersaturated waters. *J. Sediment. Petrol.* 44:7–26.

Basso, D. 2012. Carbonate production by calcareous red algae and global change. *Geodiversitas* 34:13–33.

Bittner, L., Payri, C. E., Maneveldt, G. W., Couloux, A., Cruaud, C., De Reviers, B. & Le Gall, L. 2011. Evolutionary history of the Corallinales (Corallinophycidae, Rhodophyta) inferred from nuclear, plastidial and mitochondrial genomes. *Mol. Phylog. Evol.* 61:697–713.

Bressan, G., Favretto, S., Kaleb, S. & Troma, G. 2007. Applicazione della microtomogafia computerizzata a raggi X allo studio predittivo della struttura di alghe rosse calcaree. *Biol. Mar. Mediterr.* 14:146–7.

De Choudens-Sánchez, V. & González, L. A. 2009. Calcite and aragonite precipitation under controlled instantaneous supersaturation: elucidating the role of $CaCO_3$ saturation state and Mg/Ca ratio on calcium carbonate polymorphism. *J. Sediment. Res.* 79:363–76.

Diaz-Pulido, G., Nash, M. C., Anthony, K. R., Bender, D., Opdyke, B. N., Reyes-Nivia, C. & Troitzsch, U. 2014. Greenhouse conditions induce mineralogical changes and dolomite accumulation in coralline algae on tropical reefs. *Nature comm.* 5:3310.

Farr, T. J., Broom, J., Hart, D., Neil, K. & Nelson, W. 2009. Common coralline algae of northern New Zealand: an identification guide. MIWA Information Series No. 70.

Felder, D. L., Thoma, B. P., Schmidt, W. E., Sauvage, T., Self-Krayesky, S., Chistoserdov, A., Bracken-Grissom, H. & Fredericq, S. 2014. Seaweeds and decapod crustaceans on Gulf deep banks after the Macondo Oil Spill. *Bioscience* 64:808–19.

Fredericq, S., Arakaki, N., Camacho, O., Gabriel, D., Krayesky, D., Self-Krayesky, S., Rees, G., Richards, J., Sauvage, T., Venera-Ponton, D. & Schmidt, W. E. 2014. A dynamic approach to the study of rhodoliths: a case study for the Northwestern Gulf of Mexico. *Cryptog. Algol.* 35:77–98.

Fredericq, S., Cho, T. O., Earle, S. A., Gurgel, C. F., Krayesky, D. M., Mateo-Cid, L. E., Mendoza Gonzáles, A. C., Norris, J. N. & Suárez, A. M. 2009. Seaweeds of the Gulf of Mexico. *In* Felder, D. L. & Camp, D. K. [Eds.] *Gulf of Mexico: Its Origins, Waters, and Biota. I. Biodiversity.* Texas A&M Univ. Press, College Station, Texas, pp. 187–259.

Fredericq, S. & Norris, J. N. 1995. A new order (Rhodogorgonales) and family (Rhodogorgonaceae) of red algae, which includes two calciferous tropical genera, *Renouxia* gen nov. and *Rhodogorgon. Crypt. Bot.* 5:316–31.

Harper, J. T. & Saunders, G. W. 2001. Molecular systematics of the Florideophyceae (Rhodophyta) using nuclear large and small subunit rDNA sequence data. *J. Phycol.* 37:1073–82.

Harper, J. T. & Saunders, G. W. 2002. A re-classification of the Acrochaetiales based on molecular and morphological data, and establishment of the Colaconematales ord. nov. (Florideophyceae, Rhodophyta). *Eur. J. Phycol.* 37:463–76.

Knoll, A. H., Canfield, D. W. & Konhauser, K. O. 2012. *Fundamentals of Geobiology.* Wiley-Blackwell, Chichester, UK, 464 pp.

Lanfear, R., Calcott, B., Ho, S. Y. W. & Guindon, S. 2012. PartitionFinder: combined selection of partitioning schemes and substitution models for phylogenetic Analyses. *Mol. Biol. Evol.* 29:1695–701.

Le Gall, L. & Saunders, G. W. 2007. A nuclear phylogeny of the Florideophyceae (Rhodophyta) inferred from combined EF2, small subunit and large subunit ribosomal DNA: establishing the new red algal subclass Corallinophycidae. *Mol. Phyl. Evol.* 43:1118–30.

Maddison, D. R. & Maddison, W. P. 2000. *MacClade4: Analysis of Phylogeny and Character Evolution*, Version 4.0. Sinauer Associates, Sunderland, Massachusetts.

Mateo-Cid, L. E., Mendoza-González, A. C. & García-López, D. 2014. Systematic survey of *Lithothamnion*, *Melobesia* and *Mesophyllum* species (Hapalidiaceae, Corallinales, Rhodophyta) recorded along the Atlantic coast of Mexico. *Phytotaxa* 164:226–38.

Materials Data Inc. 1224 Concannon Blvd. Livermore , CA 94550 www.MaterialsData.com

Moberly, R. 1970. Microprobe study of diagenesis in calcareous algae. 1. *Sedimentol.* 14:113–23.

Moberly, R. 1973. Rapid chamber-filling growth of marine aragonite and Mg-Calcite. *J. Sediment. Petrol.* 43:634–5.

Nash, M. C., Opdyke, B. N., Troitzsch, U., Russell, B. D., Adey, W. H., Kato, A., Diaz-Pulido, G., Brent, C., Gardner, M., Prichard, J. & Kline, D. I. 2012. Dolomite rich coral reef coralline algae resist dissolution in acidified conditions. *Nat. Clim. Change* 3:268–272.

Nash, M. C., Troitzsch, U., Opdyke, B. N., Trafford, J. M., Russell, B. D. & Kline, D. I. 2011. First discovery of dolomite and magnesite in living coralline algae and its geobiological implications. *Biogeosci.* 8:97–108.

Nash, M. C., Uthicke, S., Negri, A. P. & Cantin, N. E. 2015. Ocean acidification does not affect magnesium composition or dolomite formation in living crustose coralline algae, *Porolithon onkodes* in an experimental system. *Biogeosc. Discuss.* 12:1373–404.

Nelson, W. A. 2009. Calcified macroalgae, critical to coastal ecosystems and vulnerable to change: a review. *Mar. Freshwater Res.* 60:787–801.

Nelson, W. A., Sutherland, J. E., Farr, T. J., Hart, D. R., Neill, K. F., Kim, H. J. & Yoon, H. S. 2015. Multigene phylogenetic

analyses of New Zealand coralline algae: *Corallinapetra novaezelandiae* gen. et sp. nov. and recognition of the Hapalidiales ord. nov. *J. Phycol.*, 51:454–468.
Pardo, C., Lopez, L., Peña, V., Hernández-Kantún, J., Le Gall, L., Bárbara, I. & Barreiro, R. 2014. A multilocus species delimitation reveals a striking number of species of coralline algae forming maerl in the OSPAR maritime area. *PLoS ONE* 9:e104073.
Rambaut, A., Suchard, M. A., Xie, D. & Drummond, A. J. 2014. Tracer v1.6. Available from http://beast.bio.ed.ac.uk/Tracer.
Rasband, W. S. 1997-2014. ImageJ. U. S. National Institutes of Health, Bethesda, Maryland. Available from http://imagej.nih.gov/ij/.
Richards, J. L., Gabrielson, P. W. & Fredericq, S. 2014. New insights into the genus *Lithophyllum* (Lithophylloideae, Corallinaceae, Corallinales) from deepwater rhodolith beds offshore the NW Gulf of Mexico. *Phytotaxa* 190: 162–75.
Ronquist, F., Teslenko, M., van der Mark, P., Ayres, D. L., Darling, A., Höhna, S., Larget, B., Liu, L., Suchard, M. A. & Huelsenbeck, J. P. 2012. MrBayes 3.2: efficient Bayesian phylogenetic inference and model choice across a large model space. *Syst. Biol.* 61:539–42.
Scholle, P. S. 1978. A color illustrated guide to carbonate rock constituents, textures, cements and porosities. AAPG memoir 27, U.S. Geological Survey, the American Association to Petroleum Geologists, Tulsa, OK, USA, ISBN: 0-89181-303-9.
Seo, K. S., Cho, T. O., Park, J. S., Yang, E. C., Yoon, H. S. & Boo, S. M. 2003. Morphology, basiphyte range, and plastid DNA phylogeny of *Campylaephora borealis* stat. nov. (Ceramiaceae, Rhodophyta). *Taxon* 52:9–19.
Sherwood, A., Kurihara, A., Conklin, K., Sauvage, T. & Presting, G. 2010. The Hawaiian Rhodophyta Biodiversity Survey (2006-2010): a summary of principal findings. *BMC Plant Biol.* 10:258.
Sissini, M. N., Oliveira, M. C., Gabrielson, P. W., Robinson, N. M., Okolodkov, Y. B., Riosmena-Rodríguez, R. & Horta, P. A. 2014. *Mesophyllum erubescens* (Corallinales, Rhodophyta)—so many species in one epithet. *Phytotaxa* 190:299–319.
Smith, A. M., Sutherland, J. E., Kregting, L., Farr, T. & Winter, D. J. 2012. Phylomineralogy of the Coralline red algae: correlation of skeletal mineralogy with molecular phylogeny. *Phytochemistry* 81:97–108.
Stamatakis, A. 2006. RAxML-VI-HPC: maximum likelihood-based phylogenetic analyses with thousands of taxa and mixed models. *Bioinformatics* 22:2688–90.
Tamura, K., Peterson, D., Peterson, N., Stecher, G., Nei, M. & Kumar, S. 2011. MEGA5: molecular evolutionary genetics analysis using maximum likelihood, evolutionary distance, and maximum parsimony methods. *Mol. Biol. Evol.* 28:2731–9.
Team, R. D. C. 2010. *R: A Language and Environment for Statistical Computing*. R Foundation for Statistical Computing, Vienna, Austria. Available from http://www.R-project.org.
Thompson, J. D., Higgins, D. G. & Gibson, T. J. 1994. CLUSTAL W: improving the sensitivity of progressive multiple sequence alignment through sequence weighting, position-specific gap penalties and weight matrix choice. *Nucl. Acids Res.* 22:4673–80.
Torrano-Silva, B. N., Gomes Feirreira, S. & Oliveira, M. C. 2015. Unveiling privacy: advances in microtomography of coralline algae. *Micron* 72:34–8.
Walker, R. & Moss, B. 1984. Mode of attachment of six epilithic crustose Corallinaceae (Rhodophyta). *Phycologia* 23:321–9.
Ward's Geology Sales Catalogue. 1998. Ward's Natural Science Establishment, Inc. Research Minerals, Catalogue Item #49H5920, 73 pp.
Welch, B. L. 1947. The generalization of "Student's" problem when several different population variances are involved. *Biometrika* 34:28–35.
Woelkerling, W. J. 1988. *The Coralline Red Algae: An Analysis of Genera and Subfamilies of Nongeniculate Corallinaceae*. British Museum (Natural History), London, Oxford, UK, 268 pp.
Yang, E. C. & Boo, S. M. 2004. Evidence for two independent lineages of *Griffithsia* (Ceramiaceae, Rhodophyta) based on plastid protein-coding *psa*A, *psb*A, and *rbc*L gene sequences. *Mol. Phylog. Evol.* 31:680–8.
Yoon, H. S., Hackett, J. D. & Bhattacharya, D. 2002. A single origin of the peridinin-and fucoxanthin-containing plastids in dinoflagellates through tertiary endosymbiosis. *Proc. Natl. Acad. Sci. USA* 99:11724–9.

Supporting Information

Additional Supporting Information may be found in the online version of this article at the publisher's web site:

Figure S1. Alignment of LSU rDNA sequences analyzed in this study.

Figure S2. Phylogram showing the position of newly generated sequences (shown in bold) of *Lithothamnion* sp. 1 and sp. 2 in the Hapalidiaceae inferred from ML analyses of *psb*A sequences. Numbers above branches indicate bootstrap values out of 1,000 replicates. Scale bar indicates number of substitutions per site.

Figure S3. Phylogram showing the position of newly generated sequences (shown in bold) of *Lithothamnion* sp. 1, sp. 2, and sp. 3 in the Hapalidiaceae inferred from NJ analyses of LSU sequences. Numbers above branches indicate bootstrap values out of 2,000 replicates (values <50 not shown). Scale bar indicates number of substitutions per site.

Table S1. List of *psb*A and LSU sequences used in the phylogenetic analyses, including taxon names, GenBank accession numbers and sequence references.

Video S1. 2D video of ZEISS *X-Ray microscopy* displaying vegetative cells, filaments, conceptacles and aragonite infill in sample LAF1437A.